GA–A27340

THE ROLE OF THE RADIAL ELECTRIC FIELD, REYNOLDS STRESS AND ZONAL FLOWS IN THE L-H TRANSITION IN DIII–D

by
J.A. BOEDO, G.R. TYNAN, D.L. RUDAKOV, Z. YAN, G.R. McKEE, P. MANZ, L. SCHMITZ, R.J. GROEBNER, T.L. RHODES, G. WANG, P. DIAMOND, and the DIII–D TEAM

JUNE 2012

GENERAL ATOMICS

DISCLAIMER

GA–A27340

THE ROLE OF THE RADIAL ELECTRIC FIELD, REYNOLDS STRESS AND ZONAL FLOWS IN THE L-H TRANSITION IN DIII–D

by
J.A. BOEDO,* G.R. TYNAN,* D.L. RUDAKOV,* Z. YAN,† G.R. McKEE,† P. MANZ,*
L. SCHMITZ,‡ R.J. GROEBNER, T.L. RHODES,‡ G. WANG,‡ P. DIAMOND,*
and the DIII–D TEAM

This is a preprint of a paper to be presented at the Thirty-ninth European Physical Society Conf., on Plasma Physics, July 2–6, 2012 in Stockholm, Sweden and to be published in the *Proceedings.*

*University of California San Diego, La Jolla, California, USA.
†University of Wisconsin-Madison, Madison, Wisconsin, USA.
‡University of California Los Angeles, Los Angeles, California, USA.

Work supported in part by
the U.S. Department of Energy under
DE-FG02-07ER54917, DE-FG02-89ER53296, DE-FG02-08ER54999,
DEE-FG02-08ER54984, and DE-FC02-04ER54698

GENERAL ATOMICS PROJECT 30200
JUNE 2012

GENERAL ATOMICS

The Role of the Radial Electric Field, Reynolds Stress, and Zonal Flows in the L-H Transition in DIII-D

J.A. Boedo[1], G.R. Tynan[1], D.L. Rudakov[1], Z. Yan[2], G.R. McKee[2], P. Manz[1], L. Schmitz[3], R.J. Groebner[4], T.L. Rhodes[3], G. Wang[3], P. Diamond[1], and the DIII-D Team[4]

[1]*University of California, San Diego, 9500 Gilman Dr., La Jolla, California 92093, USA*
[2]*University of Wisconsin-Madison, 1500 Engineering Dr., Madison, Wisconsin 53706, USA*
[3]*University of California Los Angeles, PO Box 957099, Los Angeles, California 90095, USA*
[4]*General Atomics, PO Box 85608, San Diego, California 92186-5608, USA*

Data from DIII-D provide a clear correlation between increases in E_r, i.e. E_rxB, poloidal flow, electrostatic Reynolds stress (RS) ($\langle \tilde{v}_r \tilde{v}_\theta \rangle$) gradient, turbulence intensity, and poloidal velocity during limit cycle oscillations (LCOs) leading up to the H-mode transition. The RS and the E_r oscillations are slightly out of phase, consistent with causality, and they occur deeper than ~1 cm inside the LCFS. The plasma was sampled at various times during the L-LCO-H evolution. The motivation for this work is that although we understand shear-decorrelation suppression of turbulence, detailed knowledge of how that shear spontaneously develops prior to the H-mode transition, and therefore scaling, is lacking.

The L-H transition [1] in tokamak plasmas is connected to velocity shear decorrelation of turbulence [2], but the detailed process is not fully understood, involving the evolution of self-organized, turbulence-generated, large scale flows [3]. Sheared zonal flows can be generated [4] nonlinearly by the gradient of the electrostatic RS by coupling energy from higher wavenumber fluctuations to low poloidal wavenumber flows. Thus this can be viewed as a predator-prey system where the energy in the turbulence feeds zonal flows (ZFs) that in turn suppress and decorrelate the turbulence [5,6].

We use discharge conditions that tether near the L-H transition, featuring slow (1–2 kHz) oscillations, dubbed limit cycle oscillations or LCOs, that are thought to be slowed-down L-H transitions dominated by the predator-prey dynamics between large scale flows and the turbulence, eventually followed by a second transition to a quiescent H-mode. This oscillating regime has been dubbed I-phase [5].

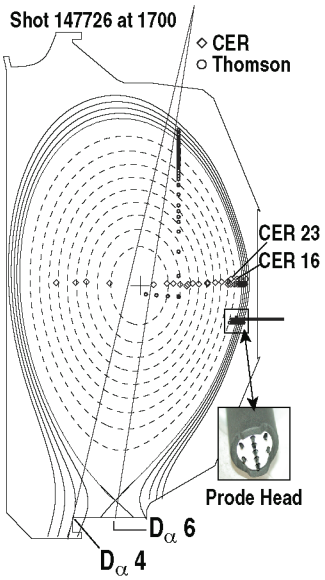

Fig. 1. LSN discharge magnetic topology showing the vertical D_α chords, Thomson scattering chords, CER chords, tangential D_α chords, and probe trajectory. Inset shows probe head.

These plasmas are obtained in DIII-D with B_T = 2.1 T, I_p = 1 MA, n_e ~ 2.7x10^{13}, P_{in} ~ 500 kW and keeping the LSN X-point at ~10 cm or less from the floor [5] as shown in Fig. 1. The time evolution of the discharge is shown in Fig. 2, with the first vertical line marking the transition into the LCO regime at

~1590 ms and the second vertical line, at ~1850 ms the final transition into H-mode. Global measures of energy and particle confinement, such as line averaged T_e and N_e and stored energy, [Fig. 2(a–c)], start increasing after the first transition, and at an accelerated rate after the second transition into a quiet H-mode. D_α measurements at the divertor [Fig. 2(d,e) and Fig. 1] show an initial fast drop into the 2 kHz oscillations for ~250 ms until the NBI input power is slightly increased [Fig. 2(c)], precipitating the second transition into H-mode. Plasma toroidal rotation and ion temperature near the edge [Fig. 2(f,g)], measured by charge exchange recombination (CER) on multiple chords (Fig. 1), increase upon entering the H-mode.

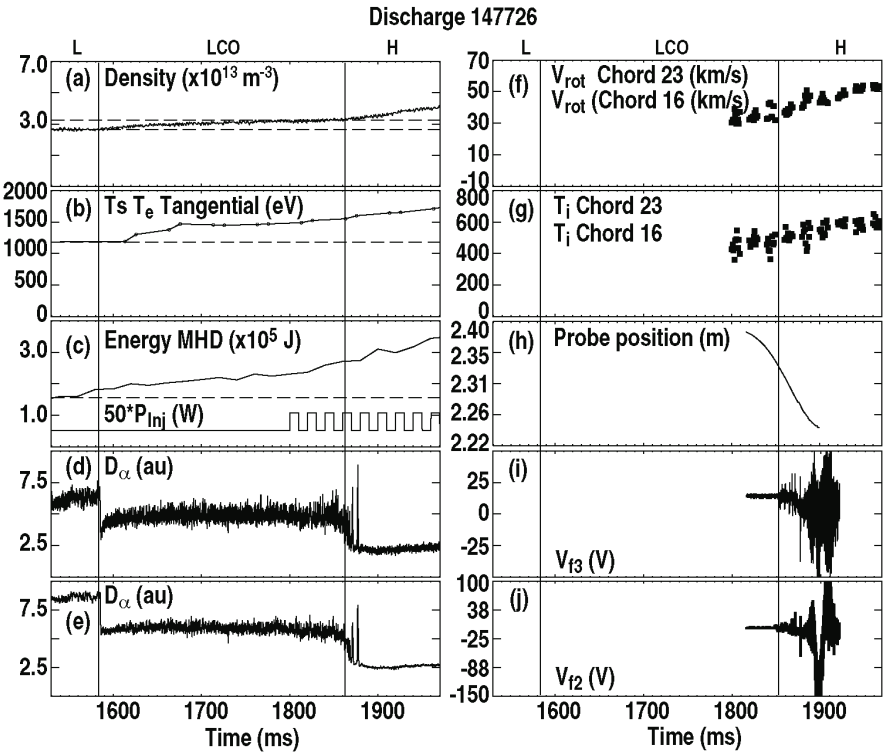

Fig. 2. Time evolution of the L-I-phase-H transition for discharge 147726, which starts at ~1590 ms, marked with the leftmost vertical bar; followed by the transition to H-mode at ~1870 ms and marked with the rightmost vertical bar. Evolution of (a) density, (b) central T_e, (c) energy content, (d,e) D_α chords at the divertor, (f) toroidal rotation near the edge, and (g) ion temperature near the edge. The probe position during the plunge is shown in (h) and two floating potential traces in (i,j).

Probe measurements were performed using a 9-pin probe array, (Fig. 1, inset), that plunges for about 150 ms [Fig. 2(h-j)] and samples various plasma parameters. The current-drawing sensors (i.e. saturation current, I_{sat}, T_e and flow measurements) were turned off in these experiments to reduce arcing, thus increasing probe plasma penetration. The focus is on obtaining multi-point plasma potential measurements V_{pl}, to deduce E_r and RS. In general (but not in this experiment), we measure T_e to estimate V_{pl} from the measurement of the floating potential, V_{fl}, obtained at various locations and combine them to get electric fields:

$$E_\theta = -\nabla_\theta V_{pl} = -\left(\frac{V_{fl}^{\theta+\partial\theta} - V_{fl}^{\theta}}{\partial\theta} \right) \quad ,$$

which is a reasonable approximation since T_e is a flux surface quantity with negligible variation over 4 mm poloidally. Similarly, we approximate E_r based on:

$$E_r = -\nabla_r V_{pl} = -\left(\frac{V_{fl}^{r+\partial r} - V_{fl}^{r}}{\partial r}\right) \approx -\left(\frac{V_{fl}^{r+\partial r} - V_{fl}^{r}}{\partial r} + 2.5 \times \frac{T_e^{r+\partial r} - T_e^{r}}{\partial r}\right) \quad .$$

We will ignore the contribution of the T_e gradient to E_r, being much smaller in L-mode than in H-mode, and assume the floating potential gradient dominates the E_r gradient, at least at the deepest probe penetration. Time records 50–100 μs long are used to calculate the fields and RMS quantities. Data is filtered below 1 kHz, low enough to eliminate low frequency components while keeping the 2 kHz oscillations of the zonal flow.

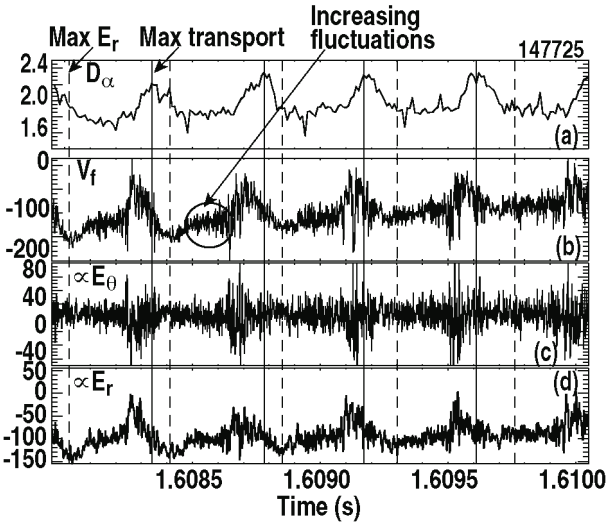

Fig. 3. Detail over a time period of 2 ms is shown: (a) D_α, (b) floating potential, (c) proxy for E_θ (not divided by d_θ), and (d) proxy for E_r (not divided by d_r). Data is taken briefly after the L-I-phase transition and mainly during the probe dwell.

Timing/causality is shown in Fig. 3 over a time span of 2 ms by comparing D_α at the divertor [Fig. 3(a)] with the floating potential, V_{fl} [Fig. 3(b)], and signals proportional to the radial and poloidal electric fields, E_r [Fig. 3(c)] and E_θ [Fig. 3(d)]. The peaks in D_α, a proxy for maximum radial transport, are preceded and accompanied by an increase in fluctuations in V_{fl} and E_θ [circled area in Fig. 3(b)] that are then quenched by the increase in E_r, which reduces the transport, and the cycle starts again.

The E_r profile (shown in Fig. 4) was measured up to ~12 mm inside the LCFS. The probe penetrates the discharge in L-mode (red) and during the dwell, the L-I transition (Fig. 2) occurs during the probe dwell in this discharge, resulting in a large increase in the average E_r from ~-6x10^3 V/m to ~-2x10^4 V/m while the LCOs, localized inside ~ -0.7 cm, occur at ~2 kHz frequency.

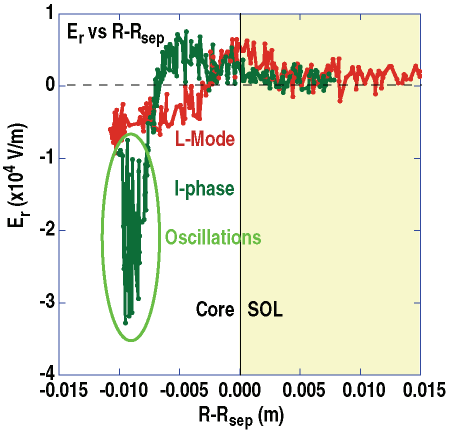

Fig. 4. Profile of approximate E_r from the probe. Probe is moving in during the L-mode and is at the dwell while the L-I-phase transition happens. The electric field oscillations are largest at about 1 cm inside the LCFS.

Direct probe measurements of RS, E_r (neglecting the T_e contribution as discussed earlier) and the fluctuations in E_θ, a proxy for radial turbulent transport are shown in Fig. 5 together with an estimate (independent of E_rxB) of the plasma poloidal velocity using time delay estimate (TDE) techniques between two poloidally separated V_{fl} measurements with the assumption that the fluctuations are frozen to the plasma.

Causality of the predator-prey system can be examined by following the time evolution of all the terms during the L-I-phase transition as shown in [Fig. 5(a-d)]. A vertical dashed line is used as a guideline. The electric field [Fig. 5(a)] grows initially, reaching and E_rxB peak velocity (at B_T = 1.5 T) is of the order of $2\text{x}10^4$ m/s and that compares well to the TDE-inferred peak velocity of ~0.5–$1\text{x}10^5$ m/s within the large scatter in the TDE calculation, due to the short records we are forced to use to properly resolve the LCOs.

The RS [Fig. 5(c)] grows and ebbs from 0.2–$1.5\text{x}10^7$ m^2s^{-2} clearly ***precedes*** the peaking in E_r which is accompanied by a drop in E_{θ}_rms [Fig. 5(d)], indicating the fluctuations are suppressed by E_r and supporting causality and the predator-prey cycle.

Consistently with the reduction in the E_θ fluctuations, global transport, reflected by D_α, increases [Fig. 3(a,c)].

In conclusion, measurements on DIII-D show that during the LCOs, the RS profile steepens by a factor of 7, followed by a deepening of the E_r well and large sheared poloidal flows of the order of 0.4–$1\text{x}10^5$ m/s that quench fluctuations and radial plasma transport. The RS profile then ebbs, followed by the shallowing of the E_r well, fluctuations grow and the process is repeated at roughly 2 kHz.

This work was supported in part by the US Department of Energy under DE-FG02-07ER54917, DE-FG02-89ER53296, DE-FG02-08ER54999, DE-FC02-04ER54698, and DE-FG02-08ER54984

[1] F. Wagner, *et al.*, Phys. Rev. Lett. **49**, 1408 (1982).
[2] H. Biglari, P. Diamond and P. Terry, Phys Fluids B **2**, 1 (1990).
[3] C. Holland *et al.*, Phys. Plasmas **14**, 056112 (2007).
[4] P.H. Diamond and Y.B. Kim. Phys. Fluids B **3**, 1626 (1991).
[5] R.J. Colchin, *et al.*, Phys. Rev. Lett. **88**, 255002 (2002).
[6] L. Schmitz, *et al.*, Phys. Rev. Lett. **108**. 155002 (2012).

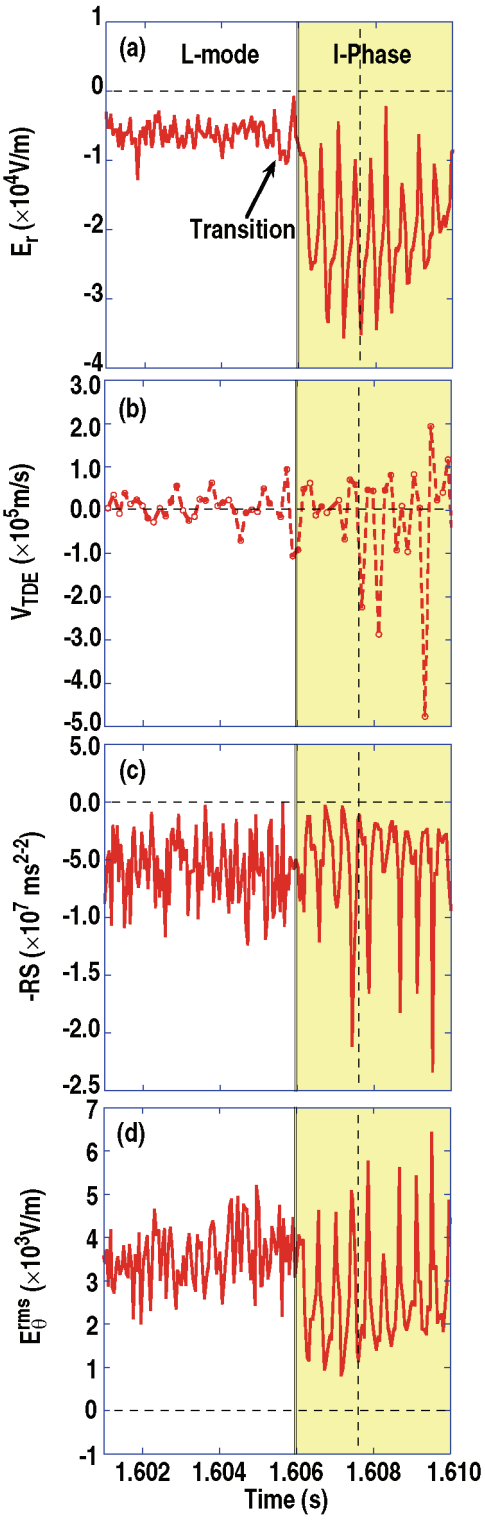

Fig. 5. The E_r oscillations (a) start as the plasma goes into the I-phase, transition indicated with a double vertical line at 1606 ms. Oscillations also shown with a vertical dashed line. (b) After the L-I-phase transition at ~1606 ms, the E_r (top) and -RS (bottom) oscillations are clearly correlated, suggesting causality.